Editor's Choice

Electronic structure, anisotropic elastic and thermal properties of the η phase Fe$_6$W$_6$C

XiaoYu Chong [a], YeHua Jiang [a,*], Rong Zhou [a], Hong Zhu [b], Jing Feng [a,c,*]

[a] Faculty of Material Science and Engineering, Kunming University of Science and Technology, Kunming 650093, People's Republic of China
[b] Department of Materials Science and Engineering, Massachusetts Institute of Technology, Cambridge, MA 02139, USA
[c] School of Engineering and Applied Sciences, Harvard University, Cambridge, MA 02138, USA

ARTICLE INFO

ABSTRACT

The optimized structure, chemical bonding characteristics, elastic and thermal properties of Fe$_6$W$_6$C are investigated by the first principle calculations with and without dispersion-corrected methods combined with the quasi-harmonic approximation. The bonding behaviors of Fe$_6$W$_6$C are discussed by the density of states and Mulliken population analysis. Anisotropy of shear and Young's moduli are characterized by three-dimensional surface contours and the planar projections on different planes. Anisotropy of the minimum thermal conductivity of Fe$_6$W$_6$C is discussed based on Cahill's model and Clarke's model and the values are 1.38 and 1.26 W m^{-1} K^{-1} predicted by these two models. Moreover, the 3D representation of the anisotropic thermal conductivity of Fe$_6$W$_6$C is obtained based on the Clarke's model and anisotropic Young's modulus.

1. Introduction

The tungsten-containing η-carbides Fe$_3$W$_3$C, Co$_3$W$_3$C, Co$_6$W$_6$C and Fe$_6$W$_6$C, etc. possess interesting properties as refractory and hard materials, and recently as potential catalysts. These phases could occur at the interfaces in heterogeneous composite materials, i.e., the interfaces between WC and transition metals (or their alloys) or tungsten-containing steels as secondary phases [1,2]. These compounds can also be prepared using special synthetic routes such as mechanical alloying [3]. Among the several phases, Fe$_6$W$_6$C is an important one and has attracted much attention to be investigated. Waki et al. systematically studied electronic properties of the η-carbide-type compounds, synthesized the Fe$_6$W$_6$C compounds and measured its magnetic susceptibility [4]. Suetin et al. investigated the structural, electronic, magnetic properties and stability of η carbides by first-principles FLAPW-GGA calculations [5]. Liu et al. explored the stability, electronic and mechanical properties of Fe–W–C system [6]. But as a common phase in the interface region of WC/Fe composites, a good understanding on thermodynamic and elastic properties of Fe$_6$W$_6$C is important to

better control and improve the properties of the composites. In this paper, both the density functional theory and quasi-harmonic approximation are employed to obtain the anisotropic elastic and thermal properties of Fe$_6$W$_6$C.

2. Methods and details

The first-principles calculations based on the density functional theory (DFT) are implemented in Cambridge Serial Total Energy Package (CASTEP) code, with a plane-wave cutoff energy of 400 eV and a $6 \times 6 \times 6$ Monkhorst–Pack k-point grid. Ultra-soft pseudo potentials (USPPs) are used to represent the interactions between ionic cores and valence electrons. The Broydene–Fletchere–Goldarbe–Shanno (BFGS) method is applied to optimize the crystal structure until the total energy changes are converged to 1×10^{-6} eV and the forces per atom are less than 0.02 eV/Å [7]. In this work, generalized gradient approximation (GGA) within two different functional is used for exchange–correlation energy calculations. One is the Perdew, Burke and Ernzerhof approach [8] and the other one is the Perdew and Wang parameterization (PW91) combined with the OBS method for the calculations of dispersion interactions such as the Van Der Waals (VDW) interactions [9]. The elastic properties are determined using the stress–strain relations by deforming the unit cell. The density functional theory (DFT) method combined with the quasi-harmonic approximation (QHA) and Debye model is used to calculate the thermodynamic

* Corresponding authors at: Faculty of Material Science and Engineering, Kunming University of Science and Technology, Kunming 650093, People's Republic of China (Y. Jiang), School of Engineering and Applied Sciences, Harvard University, Cambridge, MA 02138, USA. Tel.: +1 6174964295; fax: +1 857 259 2445 (J. Feng).
E-mail addresses: jiangyehua@kmust.edu.cn (Y. Jiang), jfeng@seas.harvard.edu (J. Feng).
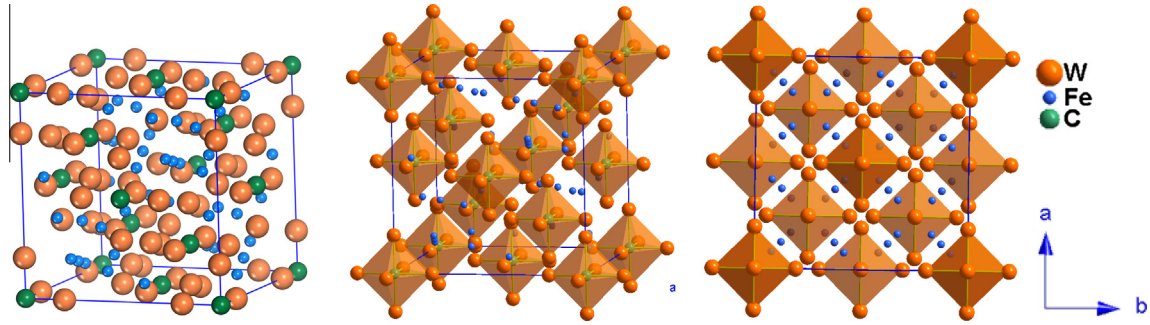
Fig. 1. Crystal structure of Fe_6W_6C. The large orange ball, medium green ball and small blue ball represent the tungsten atom, carbon atom and iron atom, respectively. (For interpretation of the references to color in this figure legend, the reader is referred to the web version of this article.)

properties of Fe_6W_6C at finite temperatures. The studied crystal structure of Fe_6W_6C is shown in Fig. 1. The type of lattice of Fe_6W_6C belongs to the complex cubic structure and the space group is FD−3M. The unit cell contains 48 iron atoms, 48 tungsten atoms and 8 carbon atoms, in which the C atoms occupy the octahedral interstice of W atoms and the strong W–C bonds surround the Fe atoms.

3. Results and discussions

3.1. Equilibrium crystal parameters and mechanical modulus

The calculated equilibrium lattice parameters are shown in Table 1, together with the experimental and other theoretical results [5,10]. From Table 1, it is clearly seen that the calculated results are close to experimental ones. The lattice constants calculated using PW91 functional combined with the dispersion-corrected method are a little smaller than the results obtained from other methods. The tiny difference between experimental and theoretical results can be attributed to the thermodynamic effects on the crystal and the lattice defect. The obtained elastic constants and mechanical modulus evaluated within Viogt–Reuss–Hill approximation are summarized in Table 2. It is obvious that the mechanical parameters estimated using PW91 functional and OBS method are larger than that obtained with PBE functional. Furthermore, the bulk (B) and shear modulus (G) of Fe_6W_6C are all smaller than that of h-WC (393.0 and 286.2 GPa), but equivalent to h-W_2C (330.6 and 190.6 GPa) [11]. The value of B/G and Poisson's ratio (σ) are calculated within the common expression [12], which are all larger than the critical value (1.75 and 0.26), indicating Fe_6W_6C is more ductile than other transition metal carbides ceramic such as h-WC (1.37 and 0.21) [11], VC (1.53 and 0.23) [12] and TiC (1.22 and 0.18) [13]. The transverse and longitudinal sound velocities (v_t and v_l), mean sound velocity (v_m), Debye temperature (Θ_D) are also evaluated in this work using the following relations in order to calculate the thermal conductivity in the next part.

$$\Theta_D = \frac{h}{k_B}\left[\frac{3n}{4\pi}\left(\frac{N_A\rho}{M}\right)\right]^{1/3} v_m \qquad (1)$$

$$v_m = \left[\frac{1}{3}\left(\frac{2}{v_t^3}+\frac{1}{v_l^3}\right)\right]^{-1/3} \qquad (2)$$

$$v_l = \sqrt{\frac{(B+(4/3)G)}{\rho}} \qquad (3)$$

$$v_t = \sqrt{\frac{G}{\rho}} \qquad (4)$$

here h is the Planck's constant, k_B is the Boltzmann constant, N_A is the Avagadro's constant, n is the number of atoms per formula, M is the molecular weight, ρ is the theoretical density of the compound. The calculated results are shown in Table 2. Moreover, the lattice parameters and bulk modulus as the function of temperature are obtained from the fitting of the Birch–Murnaghan equation of state [14] and QHA approximation, which is presented in Fig. 2. The effects of thermal energies on the lattice parameter and bulk modulus are caused mainly by lattice vibrations or phonons. With the temperature increasing from 0 K to 1200 K, the lattice parameter rises from 10.871 to 10.886 Å and the bulk modulus decreases from 327.8 to 326.7 GPa, suggesting the strong thermal stability for Fe_6W_6C.

3.2. Heat capacity and thermal expansion coefficient

In order to study the thermal properties of Fe_6W_6C, the volume dependence of total energy is obtained by the DFT calculations. The heat capacity at constant pressure (C_p) can be achieved by analyzing the phonon frequencies of the crystal structure and the Debye model is applied to evaluate the heat capacity at constant volume (C_V) [15]. Then the calculated difference between the two heat capacities can be correlated to thermal expansion and temperature through $C_P(T) - C_V(T) = \beta^2 V(T) T B_0(T)$ [16], where β is volumetric thermal expansion coefficient; $V(T)$ is the equilibrium cell volume at temperature T obtained from lattice parameter and $B_0(T)$ is the isothermal bulk modulus which have been calculated in the previous part. For cubic crystal class, the linear expansion coefficient (α)

Table 1
Lattice parameters of the studied Fe_6W_6C structure determined both by experiment and theoretical calculation.

| Method	Lattice constants (Å)			Lattice angles (°)			ρ (g/cm³)	V (Å³)	Reference
	a	b	c	α	β	γ			
GGA-PW91 + OBS	10.81	10.81	10.81	90	90	90	15.24	1264.5	This work
GGA-PBE	10.87	10.87	10.87	90	90	90	15.00	1284.0	This work
EOS	10.87	10.87	10.87	90	90	90	15.00	1284.7	This work
FLAPW-GGA-PBE	10.90	10.90	10.90	90	90	90	14.87	1295.2	[5]
Experiment	10.93	10.93	10.93	90	90	90	14.73	1307.2	[11]

Table 2
Elastic constants (GPa), mechanical modulus (GPa), Poisson's ratio, acoustic velocities and Debye temperature for Fe_6W_6C.

Method	C_{ij}			B	G	E	B/G	σ	v_l	v_t	v_m	Θ_D
	C_{11}	C_{44}	C_{12}									
GGA-PW91+OBS	609.6	173.7	204.8	339.8	184.7	469.0	1.84	0.27	6201	3481	3874	501.5
GGA-PBE	593.5	168.0	203.9	333.8	178.3	454.0	1.87	0.27	6172	3447	3838	494.2
EOS				327.8								
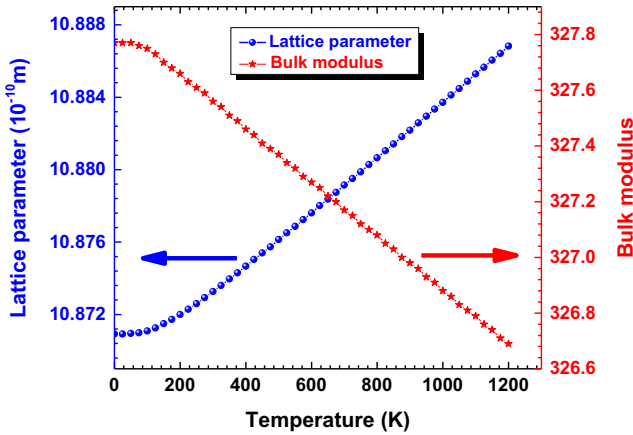
Fig. 2. Temperature dependence of lattice parameter and bulk modulus of Fe_6W_6C.

and volumetric coefficient are related by $\beta = 3\alpha$ [16]. All the results can be found in Fig. 3. From Fig. 3(b) and (c), we can clearly find that the C_V and C_p of Fe_6W_6C increase sharply below the Debye temperature (501.5 K), but above the Debye temperature, C_V and C_p increase linearly as a function of temperature and the C_V approaches to a constant which is well described by the classic Dulong–Petti rule, i.e., 3NR, at very high temperature. For Fe_6W_6C, the value is 324.25 J mol^{-1} K^{-1}.

The thermal expansion characterizes the anharmonic lattice vibrations of a crystal. The calculated linear expansion coefficient (α) is shown in Fig. 3(d), which exhibits similar variation tendency as C_V and C_p. The propensity of increment of α becomes very moderate at high temperature, which means that α changes slowly and increases linearly with respect to temperature. For Fe_6W_6C, the α value approach 7.53×10^{-6} K^{-1} at 1200 K, indicating that it is thermal expansion coefficient is low compared with the steel and iron materials.
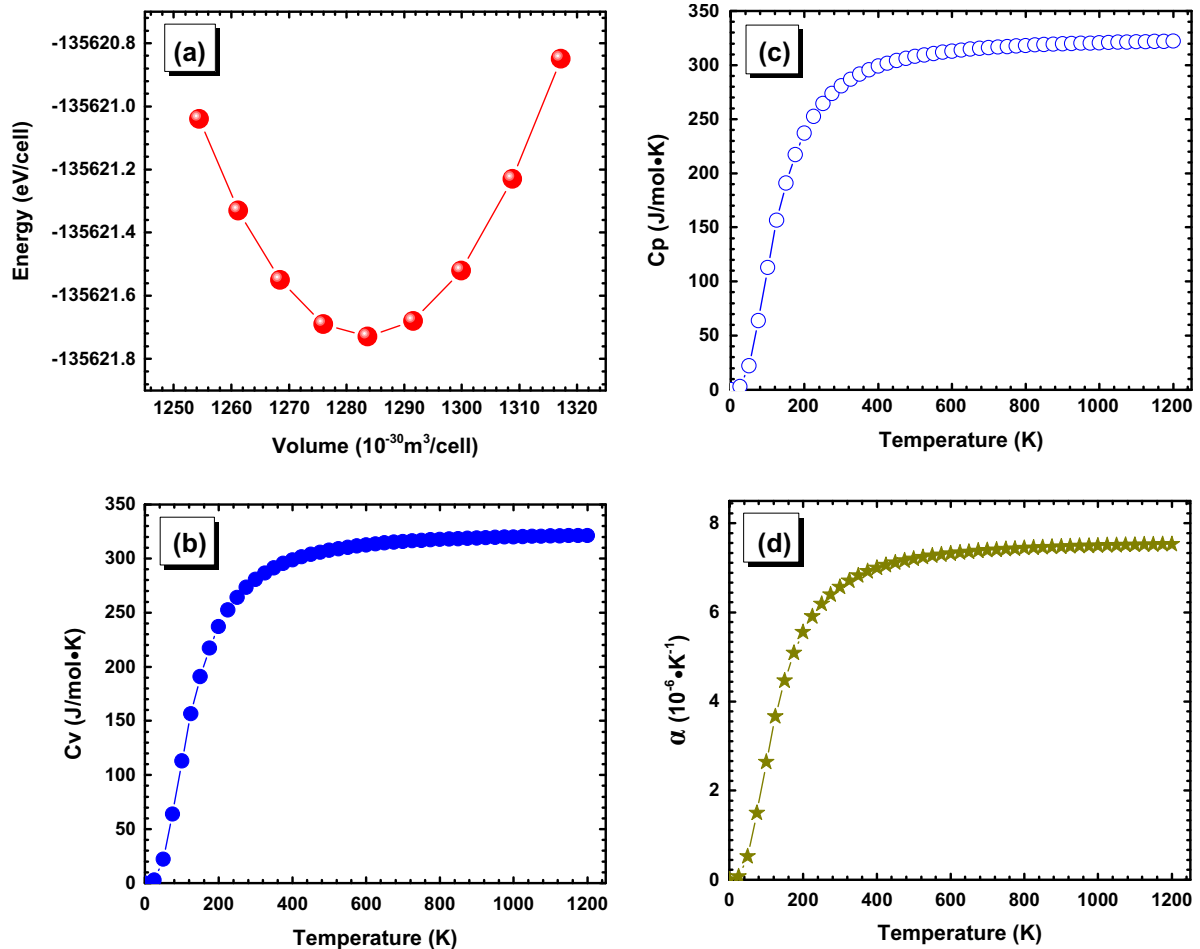
Fig. 3. The curve of the volume dependence of total energy (a); the temperature dependence of C_V, C_p and α (b)–(d).
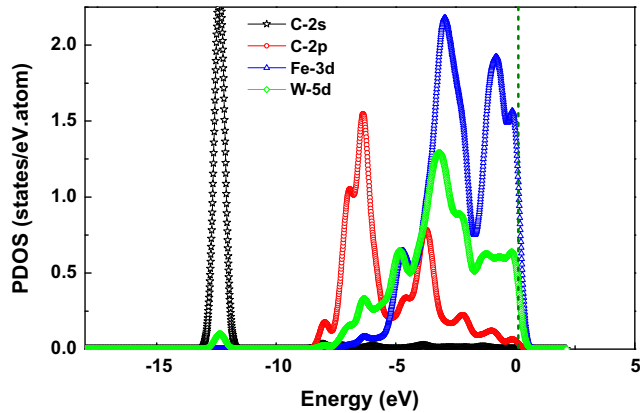
Fig. 4. The partial density of states (PDOS) for Fe_6W_6C. The dash line represents the Fermi energy.

3.3. Electronic structure

In order to reveal the electronic origin of the calculated properties of Fe_6W_6C, the density of states (DOS) and electron density distribution maps are calculated and plotted in Figs. 4 and 5, respectively. From Fig. 4, we can clearly see that Fe_6W_6C is an insulator. The d bands of metal atoms dominate the Fermi level. Furthermore, the 3d band of Fe and 5d band of W are overlapped with the 2p band of C near Fermi level, implying the covalent interactions between the C and metal atoms by *p–d* hybridization and the metallic bonding between metal atoms. So the bonding behaviors of Fe_6W_6C are the combinations of covalent and metallic bonds. Another evidence can be found in Fig. 5(a), in which the core regions for all the W, Fe and C have large values and smaller in interstitial area. Covalent bond features can be seen clearly in the picture between W and C atoms, and interactions of metallic bonds between Fe and W are also evidence. More details can be found from electron density difference distribution in Fig. 5(b). Some electrons are delocalized and distributed through the matrix map in the area between Fe and W atoms, suggesting the characteristics of metallic bonding. The electrons in the blue color area are effectively localized around the C atoms and strong polarized covalent bonds can be concluded between W and C atoms. The large mechanical modulus and low thermal expansion coefficient can be attributed to the strong bonding between W and C atoms.

The Mulliken population analysis on the chemical bonds of Fe_6W_6C is conducted by DFT calculations with the GGA-PBE functional, as shown in Fig. 6. The Mulliken populations of W–C bonds are higher than those of other bonds, indicating high level of covalency of bonds. There is only one type C–W bond in CW_6 octahedron, while two different bond lengths and Mulliken populations exist in Fe–Fe and Fe–W bonds. Moreover, the bond lengths as well as the Mulliken population of C–W bonds are quite different from those of Fe–W and Fe–Fe bonds, which demonstrate anisotropic chemical bonding nature of Fe_6W_6C. The lengths of metallic bonds are longer and the Mulliken populations are smaller than those of C–W bonds, implying that metallic bonds are weaker than C–W bonds. In general, Fe_6W_6C show heterogeneous bonding nature and complex structures. These structural features play an essential role in the properties and performances of these two materials.

3.4. Anisotropy of mechanical modulus and thermal conductivity

The calculated elastic compliance constants and anisotropic index are summarized in Table 3. For the universal anisotropic index (A^U) and percent anisotropic index (A_B and A_G), the large

discrepancies from zero refer to the highly mechanical anisotropic properties and the values of A_1, A_2 and A_3 should be one for an isotropic crystal [17]. From the A_B value we can conclude that the bulk modulus is isotropic for Fe_6W_6C. But the Young's modulus is more dependent on the direction which is confirmed by A_B and A_G values. A_1, A_2 and A_3 values are 0.86 for Fe_6W_6C, indicating that Fe_6W_6C has weak anisotropy of shear modulus.

Another more intuitive and simple way to describe the anisotropic behavior of elastic properties for Fe_6W_6C is to plot the three-dimensional (3D) surface contour for mechanical modulus in spherical coordinates as a function of the crystallographic orientation. For the shear modulus, the shear stress direction and the shear plane must be considered in the 3D coordinate, which make it difficult to draw the 3D anisotropic picture of shear modulus. In this paper, the anisotropy of torsion shear modulus for Fe_6W_6C (G_T) is discussed to solve the problem. The directional dependence of torsion shear modulus and Young's modulus is given by [18,19]:

$$\frac{1}{G_T} = S_{44} + 4\left[(S_{11} - S_{12}) - \frac{1}{2}S_{44}\right](l_1^2 l_2^2 + l_2^2 l_3^2 + l_1^2 l_3^2) \quad (5)$$

$$\frac{1}{E} = l_1^4 S_{11} + l_2^4 S_{22} + l_3^4 S_{33} + 2l_1^2 l_2^2 S_{12} + 2l_1^2 l_3^2 S_{13} + 2l_2^2 l_3^2 S_{23} \\ + l_1^2 l_2^2 S_{66} + l_1^2 l_3^2 S_{55} + l_2^2 l_3^2 S_{44} \quad (6)$$

where S_{ij} is the elastic compliance constants and l_1, l_2 and l_3 are the directional cosines ($l_1 = \sin\theta\cos\varphi$, $l_2 = \sin\theta\sin\varphi$, $l_3 = \cos\varphi$). The obtained contour images are shown in Fig. 6(a) and (b). For an isotropic crystal, a sphere is anticipated. As we can see from Fig. 7, Young's modulus of Fe_6W_6C has stronger directional dependence than shear modulus. Projections of Young's modulus on the (0 0 1) and (1 1 0) planes for Fe_6W_6C are also shown in Fig. 6(d), which are all deviated from the regular ellipses. The shapes of planar contours on (0 0 1) and (1 1 0) planes are alike and show the maximum Young's modulus as 506.6 GPa along [0 1 0] and [0 0 1] directions, respectively. Moreover, the minimum Young's modulus for Fe_6W_6C on (0 0 1) and (1 1 0) planes are 459.1 and 445.2 GPa.

The anisotropy of the minimum thermal conductivity for Fe_6W_6C is now addressed based on Cahill's model and Clarke's model. Both models can give the lower limit of the thermal conductivity of a crystal. Then the thermal conductivities (κ) can be evaluated as [20,21]:

$$\text{Clark's model:} \quad \kappa_{min} = 0.87k_B\overline{M_a}^{-2/3}E^{1/2}\rho^{1/6}, \quad \overline{M_a} = [M/(m \cdot N_A)] \quad (7)$$

$$\text{Cahill's model:} \quad \kappa_{min} = \frac{k_B}{2.48}n^{2/3}(v_l + v_{t1} + v_{t2}) \quad (8)$$

where $\overline{M_a}$ is the average mass per atom, ρ is the density, M is the molar mass, m is the total number of atoms per formula, N_A is Avogadro's number, k_B is Boltzmann's constant, n is the density of number of atoms per volume, v_l is the longitudinal sound velocity, v_{t1} and v_{t2} are the transverse sound velocity. For the Clark's model, we found a simple parameter of Young's modulus (E) in it. Thus we replace the simple E with the 3D expression of anisotropy of Young's modulus (Eq. (2)) to obtain the directional dependence of the minimum thermal conductivity. The 3D surface contour of the minimum thermal conductivity of Fe_6W_6C is presented in Fig. 7(c), which can be seen that the shape of the contour is not a sphere. Furthermore, we can also plot the anisotropic minimum thermal conductivity of a crystal at different crystal planes. For Fe_6W_6C with cubic crystal, the trajectories of the minimum thermal conductivity at the (0 0 1) and (1 1 0) crystal planes are given in spherical coordinates [22]:
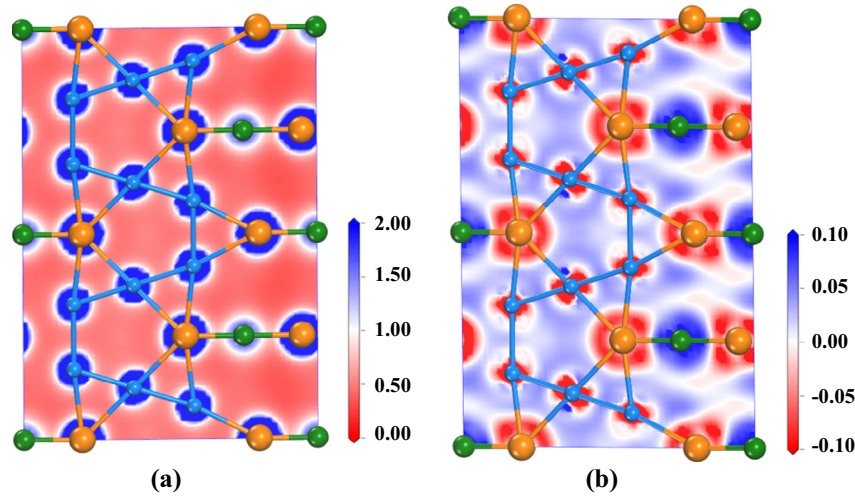
Fig. 5. Total electron density distribution contour (a) and electron density difference distribution contour (b) at (1–10) plane for Fe_6W_6C.

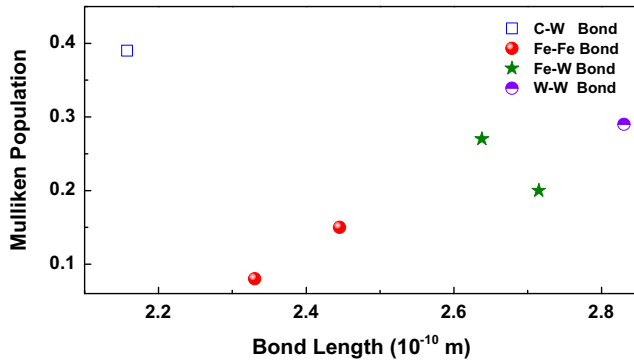**Fig. 6.** Mulliken population and bond length of chemical bonds in Fe_6W_6C.

$$\kappa_{min}^{(001)} = 0.87 k_B \overline{M_a}^{-2/3} \rho^{1/6} (S_{11}(\sin^4 \varphi + \cos^4 \varphi) + (S_{44} + 2S_{12}) \cos^2 \varphi \sin^2 \varphi)^{1/2} \quad (9)$$

$$\kappa_{min}^{(110)} = 0.87 k_B \overline{M_a}^{-2/3} \rho^{1/6} \left(S_{11} \left(\frac{1}{2} \sin^4 \theta + \cos^4 \theta \right) + (S_{44} + 2S_{12}) \left(\cos^2 \theta \sin^2 \theta + \frac{1}{4} \sin^4 \theta \right) \right)^{1/2} \quad (10)$$

The results are illustrated in Fig. 7(e) and (f). From the trajectory images one can clearly see that the minimum thermal conductivity along the [010] direction is smaller than that along other directions and the peak value ~ 1.48 W m^{-1} K^{-1} occurs along the [110] direction at the (001) plane. Furthermore, the minimum thermal conductivity close to the [1$\bar{1}$1] direction is larger than that along other directions and the minimum thermal conductivity as 1.24 W m^{-1} K^{-1} along [1$\bar{1}$0] direction is the smallest at the (110) plane.

For the Cahill's model, the sound velocities of both longitudinal and transverse waves along [100], [110] and [111] directions must be calculated using the following relations [23] to obtain the minimum thermal conductivities along different directions:

$$\text{for} \quad [100]v_l = \sqrt{C_{11}/\rho}; \quad [010]v_{t1} = [001]v_{t2} = \sqrt{C_{44}/\rho} \quad (11)$$

$$\text{for} \quad [110]v_l = \sqrt{(C_{11} + C_{12} + 2C_{44})/2\rho}; \quad [1\bar{1}0]v_{t1}$$
$$= \sqrt{(C_{11} - C_{12})/\rho}; \quad [001]v_{t2} = \sqrt{C_{44}/\rho} \quad (12)$$

$$\text{for} \quad [111]v_l = \sqrt{(C_{11} + 2C_{12} + 4C_{44})/3\rho}; \quad [11\bar{2}]v_{t1} = v_{t2}$$
$$= \sqrt{(C_{11} - C_{12} + C_{44})/3\rho} \quad (13)$$

The anisotropic sound velocities of h-WC and h-W$_2$C [24] are also quoted to estimate the thermal conductivities. All the obtained anisotropic sound velocities of Fe_6W_6C, h-WC and h-W$_2$C are shown in Table 4. The minimum thermal conductivities estimated by Clark's and Cahill's models are tabulated in Table 5. The value obtained by Cahill's model is 1.38 W m^{-1} K^{-1}, which are larger than the value 1.26 W m^{-1} K^{-1} predicted by Clark's model. The thermal conductivity of the investigated Fe_6W_6C is almost as low as that of the thermal insulators $Ln_2Zr_2O_7$ (1.2– 1.5 W m^{-1} K^{-1}), which are also evaluated by Cahill's and Clark's model and compared with the experimental results [23]. The reason is that W atom is much heavy and atomic masses and radius for W, Fe and C atoms vary widely, which may weaken the vibration of the atom and lead to different vibrational frequency for different atom. So the phonon transmission is hampered resulting in low conductivity of the crystal. As an important phase in WC/Fe composite, the thermal conductivity of Fe_6W_6C is larger than h-W$_2$C, but smaller than h-WC. Furthermore, the anisotropy of minimum thermal conductivity calculated within Cahill's model is in consistent with that estimated by Clark's model. For Cahill's model, the minimum thermal conductivity along the [110] direction is the largest among all the calculated values along different directions, which is in good agreement with the result from Clark's model.

Table 3
The calculated elastic compliance matrix (S_{ij}), universal anisotropic index (A^U), percent anisotropic index (A_B and A_G) and shear anisotropic factors (A_1, A_2 and A_3) for Fe_6W_6C.

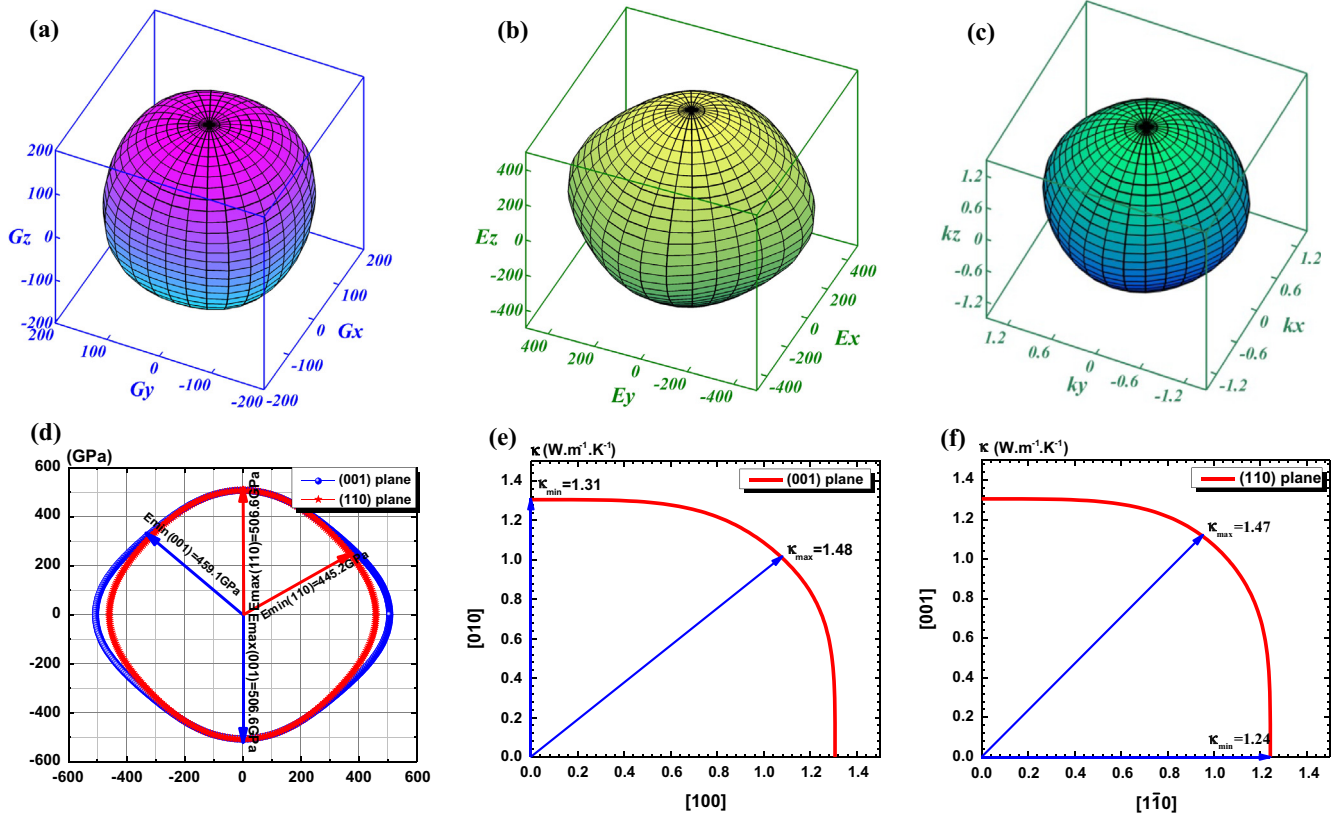| Method	S_{ij}			Shear anisotropic factors			Anisotropic index		
	S_{11}	S_{44}	S_{12}	A_1	A_2	A_3	A^U	A_B	A_G (%)
GGA-PW91+DFT-D	0.0019738	0.0057582	−0.0004964	0.86	0.86	0.86	0.02821	0	0.28
GGA-PBE	0.0020440	0.0059525	−0.0005227	0.86	0.86	0.86	0.02636	0	0.26

Fig. 7. Surface contour of anisotropic shear modulus, Young's modulus and thermal conductivity (a)–(c); planar projections of Young's modulus on (0 0 1) and (1 1 0) plane (d); the anisotropic thermal conductivities for (0 0 1) plane and (1 1 0) plane (e) and (f).

Table 4
The calculated anisotropic sound velocities of Fe$_6$W$_6$C, together with the values of h-WC and h-W$_2$C. The unit of velocity is m/s.

Species	[1 0 0]			[0 1 0]			[0 0 1]			[1 1 0]			[1 1 1]		
	v_l	v_{t1}	v_{t2}	v_l	v_{t1}	v_{t2}	v_l	v_{t1}	v_{t2}	v_l	v_{t1}	v_{t2}	v_l	v_{t1}	v_{t2}
Fe$_6$W$_6$C	6325	3376	3376	6325	3376	3376	6325	3376	3376	6174	5154	3376	6123	3557	3557
h-WC	4034	6799	4412				4412	7875	4412						
h-W$_2$C	3466	5928	3586				3586	5657	3586						

Table 5
The thermal conductivity (κ) of Fe$_6$W$_6$C, together with the values of h-WC and h-W$_2$C calculated by Clark model and Cahill's model. The unit of the minimum thermal conductivity is W m^{-1} K^{-1}.

Species	Model	M	M_a (10^{-26})	n (10^{28})	[1 0 0]κ_{min}	[0 1 0]κ_{min}	[0 0 1]κ_{min}	[1 1 0]κ_{min}	[1 1 1]κ_{min}	[1 $\bar{1}$ 0]κ_{min}	[1 $\bar{1}$ 1]κ_{min}	κ_{min}
Fe$_6$W$_6$C	Cahill			8.22	1.38	1.38	1.38	1.55	1.39			1.38
	Clark	1449.6	18.52		1.31	1.31	1.31	1.48		1.24	1.47	1.26
h-WC	Cahill			9.68	1.79		1.96					1.85
	Clark	195.8	16.26									1.68
h-W$_2$C	Cahill			7.97	1.34		1.32					1.32
	Clark	379.6	21.02									1.19

4. Conclusions

In this paper, we find that the lattice constant and bulk modulus of η phase Fe$_6$W$_6$C change slightly with the temperature increasing from 0 K and 1200 K. The heat capacity at constant pressure (C_p) and constant volume (C_V) are calculated and the C_V approaches 324.25 J mol^{-1} K^{-1} for Fe$_6$W$_6$C. The temperature dependence of linear expansion coefficient (α) for Fe$_6$W$_6$C is calculated and the value is 7.53×10^{-6} K^{-1} at 1200 K. The bonding behaviors of Fe$_6$W$_6$C are the combinations of covalent and metallic bonds. The 3D surface contour of torsion shear modulus and Young's modulus

are obtained and the anisotropy of Young's modulus of Fe$_6$W$_6$C is stronger than shear modulus. Furthermore, the 3D representation of minimum thermal conductivity of Fe$_6$W$_6$C is evaluated based on the Clark model. The minimum thermal conductivities at the (0 0 1) and (1 1 0) planes are plotted and we found that the directional dependence of thermal conductivity is determined by the anisotropy of elasticity of Fe$_6$W$_6$C. On the other hand, the anisotropy of minimum thermal conductivities is also evaluated by Cahill's model, which is in good agreement with the result from Clark's model. The κ_{min} values estimated by Cahill's and Clark's model are 1.38 and 1.26 W m^{-1} K^{-1}, respectively.

Acknowledgements

References

[1] X.Q. You, C. Zhang, X.F. Song, M.P. Huang, J.G. Ma, Appl. Surf. Sci. 253 (2007) 4409.
[2] O.O. Eso, P. Fan, Z.Z. Fang, Int. J. Refract. Met. Hard Mater. 26 (2008) 91.
[3] T. Tsuchida, N. Morita, J. Eur. Ceram. Soc. 22 (2002) 2401.
[4] T. Waki, S. Terazawa, Y. Umemoto, Y. Tabata, Y. Murase, M. Kato, K. Hirota, H. Nakamura, J. Phys: Conf. Ser. 344 (2012) 012017.
[5] D. Suetin, I. Shein, A. Ivanovskii, Physica B 404 (2009) 3544.
[6] Y.Z. Liu, Y.H. Jiang, R. Zhou, J. Feng, Comput. Mater. Sci. 82 (2014) 26.
[7] J.D. Head, M.C. Zerner, Chem. Phys. Lett. 131 (1986) 359.
[8] J.P. Perdew, K. Burke, M. Ernzerhof, Phys. Rev. Lett. 77 (1996) 3865.
[9] F. Ortmann, F. Bechstedt, W. Schmidt, Phys. Rev. B 73 (2006) 205101.
[10] J. Leciejewicz, J. Less-Common Met. 7 (1964) 318.
[11] Y.F. Li, Y.M. Gao, B. Xiao, T. Min, Z.J. Fan, S.Q. Ma, L.L. Xu, J. Alloys Compd. 502 (2010) 28.
[12] X.Y. Chong, Y.H. Jiang, R. Zhou, J. Feng, RSC Adv. 4 (2014) 44959.
[13] Y.Z. Liu, Y.H. Jiang, R. Zhou, J. Feng, J. Alloys Compd. 582 (2014) 500.
[14] F. Birch, Phys. Rev. 71 (1947) 809.
[15] J. Feng, C. Wan, B. Xiao, R. Zhou, W. Pan, D.R. Clarke, Phys. Rev. B 84 (2011) 024302.
[16] G. Grimvall, Thermophysical Properties of Materials, Elsevier, 1999.
[17] H.M. Xiang, Z.H. Feng, C.Y. Zhou, J. Eur. Ceram. Soc. 35 (2015) 1549.
[18] J.F. Nye, Physical Properties of Crystals, Clarendon Press, Oxford, 1957.
[19] H.M. Xiang, Z.H. Feng, C.Y. Zhou, J. Eur. Ceram. Soc. 34 (2014) 1809.
[20] D.R. Clarke, Surf. Coat. Technol. 163 (2003) 67.
[21] D.G. Cahill, S.K. Watson, R.O. Pohl, Phys. Rev. B 46 (1992) 6131.
[22] J. Feng, B. Xiao, R. Zhou, W. Pan, Scripta Mater. 68 (2013) 727.
[23] J. Feng, B. Xiao, C.L. Wan, Z.X. Qu, Z.C. Huang, J.C. Chen, R. Zhou, W. Pan, Acta Mater. 59 (2011) 1742.
[24] Y.Z. Liu, Y.H. Jiang, R. Zhou, J. Feng, Ceram. Int. 40 (2014) 2891.